Observation of tidal deformations in a tectonically active region of the Northern Caucasus

Vadim K. Milyukov[a*], Alexander V. Kopaev[a], Anna V. Lagutkina[a], Alexey P. Mironov[a], Andrey V. Myasnikov[a], Boris S. Klyachko[a]

[a]Sternberg Astronomical Institute, Moscow State University, Russia.

The results of observations of tidal strains of the crust observed in a mountainous area of the Northern Caucasus near to the volcano Elbrus during the period 2003–08 are presented. Precise crustal strain observations are carried out using the Baksan laser interferometer strainmeter with a measuring arm length of 75 m and resolution of 2.3×10^{-13}. The four-year record is characterized by remarkable annual strain changes of the order of $(1 - 1.5) \times 10^{-6}$ and linear strain accumulation of -3.74×10^{-7} /year. Harmonic analysis, performed with the help of the `ETERNA` software package, reveals temporal variations in the amplitude factors of the main tidal waves M_2 (within 1.02–1.15) and O_1 (within 0.76–1.24). The influence of the topography on tidal strains in the Baksan gorge is estimated at 22% (an increase in the measured strain values). Therefore the reduced amplitude factors of the main diurnal and semidiurnal waves are underestimated. Numerical modeling of tidal anomalies produced by regional heterogeneous inclusions is performed in a *2-D approximation*. The observed anomaly of the M_2 wave (12%) is shown to be due to the influence of the main magma-controlling fault associated with the deep magma source of the Elbrus dormant volcano. The preliminary analysis of the evidence of *the fluid core resonance* (FCR) effect in the diurnal tidal band has been carried out.

Keywords: Earth tides; crustal deformations; volcano structures

1. Introduction

The northern part of the Greater Caucasus is one of the most geodynamically active regions of Russia [11]. From the standpoint of modern geodynamics, this region represents a typical example of collision tectonics, characterized by the accumulation of compressive deformations in the submeridional direction, extension in the sublatitudinal direction, and the continuing overall uplift of the Greater Caucasus mountain system, that is still occurring. This is a zone of complex tectonics associated with the interaction of two of the Earth's major lithospheric plates, Arabia and Eurasia. Therefore, the region as a whole is characterized by a complex system of faults with meridional and diagonal structures.

The Elbrus volcanic center, located on the northern slope of the main range of the Greater Caucasus, is the highest point of Europe. The west top has an altitude of 5643

*Postal address: Sternberg Astronomical Institute of Lomonosov Moscow State University, 13, Universitetskij prospekt, Moscow, 119992, Russia; Phone: (495) 939 1634; Fax: (495) 932 8841; E-mail: milyukov@sai.msu.ru

m and the east top has an altitude of 5620 m. Mount Elbrus is classified as an active volcano with previous historical eruptions clearly dated to the Holocene. Current classifications define Elbrus as a dormant volcano that could become active even after millennia of quiescence [1]. Recent geological–geophysical investigations conducted in the Elbrus region found that a significant volume of low-density substance with a temperature of at least 700°C could exist beneath the volcano at a depth of about 20–30 km. This volume could potentially have been the magma source that supplied the material for previous eruptions of Mount Elbrus [2].

In this unique place for studying geodynamic and volcanic processes, the geodynamic observatory of the Sternberg Astronomical Institute of Moscow University has been created. The Baksan geodynamic observatory is located in the Elbrus area (Baksan gorge) of the Kabardino-Balkaria region 30 km southwest of the town of Tyrnyauz; the distance of the observatory from Elbrus volcano is 18 km. The long-term monitoring of lithosphere deformations of this region is carried out by the long-base laser interferometer–strainmeter.

A horizontal strainmeter oriented at an arbitrary azimuth α measures the following combination of strain components [4]:

$$\varepsilon_{obs} = \varepsilon_{\theta\theta}\cos^2\alpha + \varepsilon_{\varphi\varphi}\sin^2\alpha + \varepsilon_{\theta\varphi}\sin 2\alpha \ , \tag{1}$$

were

$$\begin{aligned}
\varepsilon_{\theta\theta} &= \frac{1}{gr}\left(hW_2 + l\frac{\partial^2 W_2}{\partial\theta^2}\right) \ , \\
\varepsilon_{\varphi\varphi} &= \frac{1}{gr}\left(hW_2 + l\cos\theta\frac{\partial W_2}{\partial\theta} + \frac{l}{\sin^2\theta}\frac{\partial^2 W_2}{\partial\varphi^2}\right) \ , \\
\varepsilon_{\theta\varphi} &= \frac{1}{gr}\left(\frac{l}{\sin\theta}\frac{\partial^2 W_2}{\partial\theta\partial\varphi} - l\frac{\cos\theta}{\sin\theta}\frac{\partial W_2}{\partial\varphi}\right) \ .
\end{aligned} \tag{2}$$

The Love number $h = 0.61$ and the Shida constant $l = 0.08$ are determined from the solution of the problem of the forced oscillations in a spherically symmetric model of an elastic Earth (the preliminary reference Earth model [3]) under the action of the lunisolar potential W_2; g is the gravity at the Earth's surface.

It is well known that the observed amplitudes of tidal strains can differ significantly from theoretical amplitudes calculated for the accepted model of the Earth. These anomalies are mainly controlled by the structure and elastic characteristics of the crust and upper mantle, in particular by the presence of deep faults or other heterogeneous inclusions near observation points, as well as by the topography, especially in mountainous areas. The role of such heterogeneous inclusions can be played, in particular, by the magmatic structures of the volcano Elbrus.

This study presents the results of long-term tidal strain observations made with the Baksan laser interferometer strainmeter. The observed amplitude anomaly of the tidal wave M_2 is interpreted in the framework of the existence of regional low-density inclusions which can be associated with the magmatic structure of the volcano Elbrus. Finally, we use the whole data to estimate the effect of *the fluid core resonance* (FCR) on the amplitudes of diurnal tidal harmonics.

2. Baksan laser interferometer

The Baksan laser interferometer is a Michelson two-beam unequal-arm interferometer operating in the regime of separated beams. The length of its larger (measuring) arm is L = 75 m (accordingly, its optical length is 150 m), and the length of the minor (reference) arm is 0.3 m. The optical elements of the interferometer are mounted in two cylindrical vacuum chambers whose lower parts are built into pedestals. The supporting pedestals of the interferometer are concrete pillars deepened to 1.5 m, rigidly connected with bedrock, and protruding beyond the lower level of the gallery for 30 cm. The chambers are connected to each other by three bellows and vacuum tubes 30 cm in diameter that form a light guide (Fig. 1). In a stationary regime, the pressure in the system is 10^{-2} Pa. An electronic recording system ensures operation of the interferometer in a wide range of frequencies, from ultralow (limited only by the time interval of continuous observations) to thousands of hertz. In a standard regime, the lithospheric strains are monitored by five frequency channels. The instrumental resolution of the interferometer is 2.3×10^{-13} for crustal strain measurement. The design and technical layout of the Baksan interferometer are described in detail in [6] and [5].

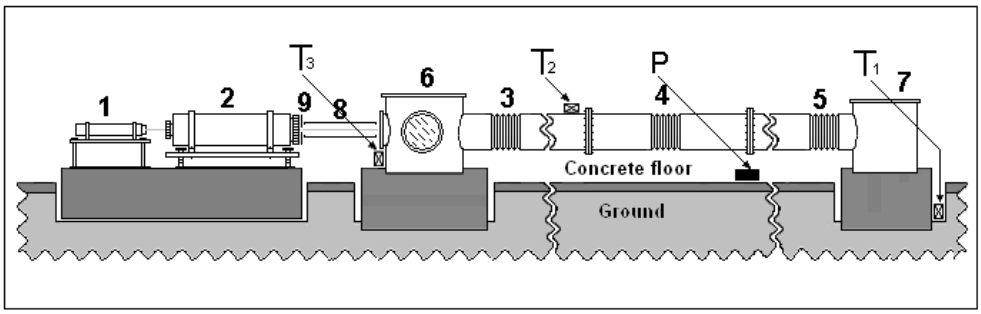

Figure 1. General scheme of the Baksan laser interferometer and the position of monitoring sensors: (1, 2, 8, 9) laser, telescopic system and light guide; (3, 4, 5) bellows; (6, 7) vacuum chambers; (T_1, T_2, T_3) temperature sensors; (P) pressure gauge.

The interferometer is mounted at a level of 650 m and a depth of 400 m inside the main gallery of the Baksan Neutrino Observatory, Institute of Nuclear Research (INR), Russian Academy of Sciences (RAS). The coordinates of the interferometer are (43°12′N, 42°43′E), and its azimuth is 150°37′. The temperature of the interferometer units and environment is monitored by three sensors with a resolution of 0.005°C. The sensors T_1, T_2, and T_3 (Fig. 1) are installed on the concrete basement below the gallery floor level, on the light guide surface, and in the lower part of the vacuum chamber, respectively. The atmospheric pressure is recorded by the gauge P of the membrane type with a resolution of 2.7 mPa. The pressure inside the interferometer is monitored by a vacuum electric-discharge magnetic gauge.

3. Observations and data analysis

Long-term monitoring of the crustal deformation is being carried out over a period of ten years. The results of four years observations of hourly variations in strains, "rock" temperature (T_1 sensor), and atmospheric pressure are shown in Fig. 2. Thirty day running means are superposed on the temperature and pressure curves. The increase in temperature is displayed downward. As shown in Fig. 2, the strain record is characterized by remarkable annual changes of the order of $(1-1.5)\times10^{-6}$ and linear strain accumulation of -3.74×10^{-7} /year. The annual strain changes are inversely proportional to "rock" temperature changes.

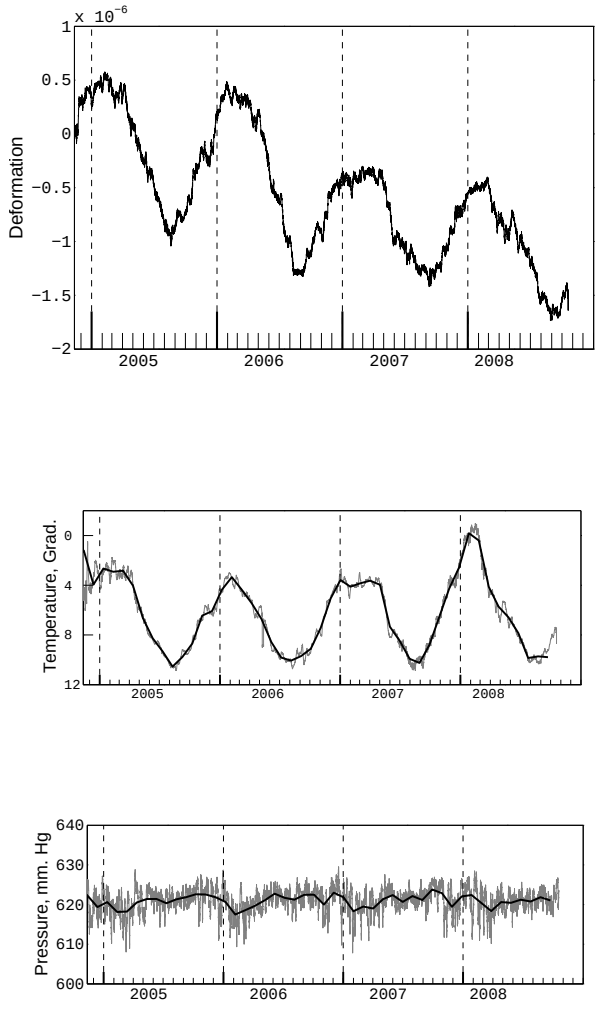

Figure 2. Observational results of strain (a), "rock" temperature (b) and atmospheric pressure (c) changes during the period from November 2004 to October 2008 (the temperature scale is inverted).

Records of crustal strains, atmospheric pressure, and temperature variations during the period 2003–08 were used for harmonic analysis. The data are represented as two periods of continuous observations: September 2003 – May 2004 and November 2004 – August 2008. The periods were divided into 53 monthly segments. An example of observed monthly data filtered in tidal frequency band is shown in Fig. 3. The diurnal and semidiurnal groups of tidal waves revealed by the Fourier analysis of all data are shown in Fig. 4.

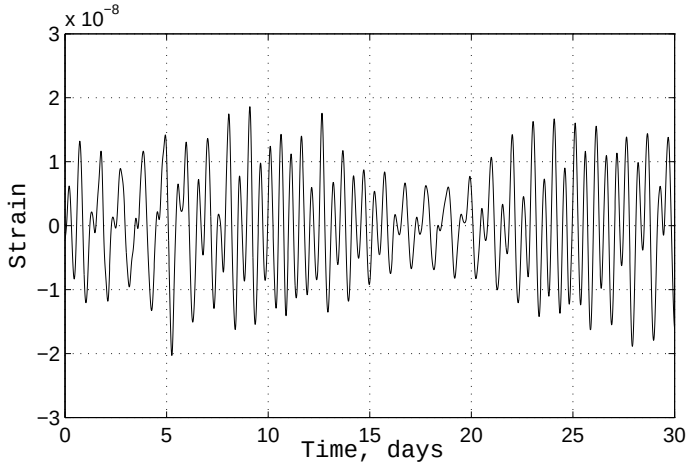

Figure 3. One month observed tidal data.

Harmonic analysis of a one-month series of observations was performed with the use of the ETERNA software package. The decomposition included eleven groups of tidal harmonics: six in the diurnal range (Q_1, O_1, NO_1, $P_1S_1K_1$, J_1, OO_1) and five in the semidiurnal range ($2N_2$, N_2, M_2, L_2, S_2K_2). The waves P_1, S_1 and K_1 and the waves S_2 and K_2 are united in two groups because they cannot be determined separately from one-month intervals of observations. ETERNA allows the calculation of the regression of strain data for various meteorological parameters. The temperature regression was calculated for each of the three temperature channels. We examined the dependence of the calculated results on the temperature channel used. The signal-to-noise ratio for the main tidal waves M_2 and O_1 was a criterion of the efficiency of compensation for the temperature dependence. The largest values of the signal-to-noise ratio are obtained for data for the channel T_2, reflecting well the diurnal temperature variations.

The results of monthly harmonic analysis of the tidal waves O_1 and M_2 are presented next (Fig. 5). The signal-to-noise ratios for the main lunar diurnal wave O_1 vary from 15 to 70 (on average, 30). The determination uncertainty of the amplitude factor is 2–5%. The main lunar semidiurnal wave M_2 has a signal-to-noise ratio within the range 70–280 (on average, 150). The determination uncertainty of the amplitude factor is 0.4–1%. The lower signal-to-noise ratio for the O_1 wave is evidently due to the presence of a residual

a) **b)**

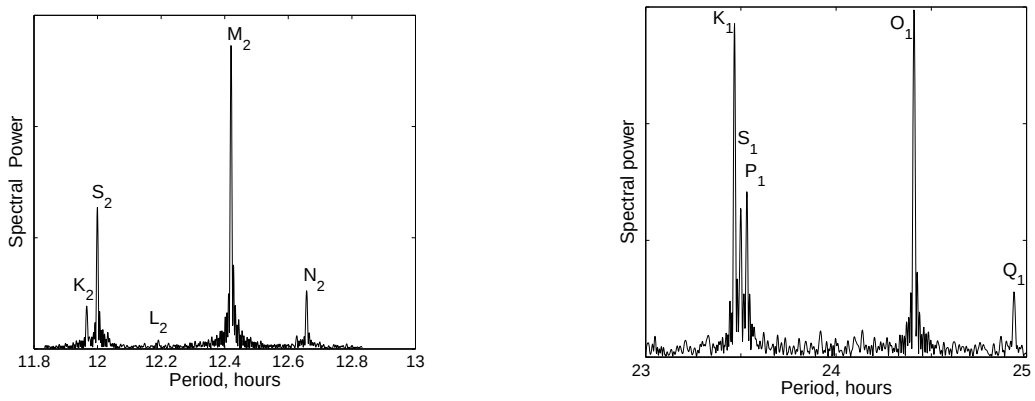

Figure 4. Spectra of (a) the semidiurnal and (b) diurnal groups of tidal waves.

a)

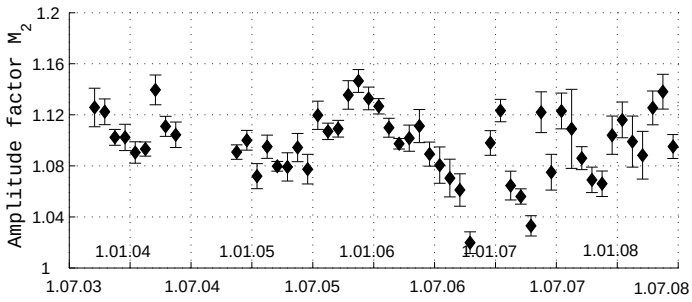

b)

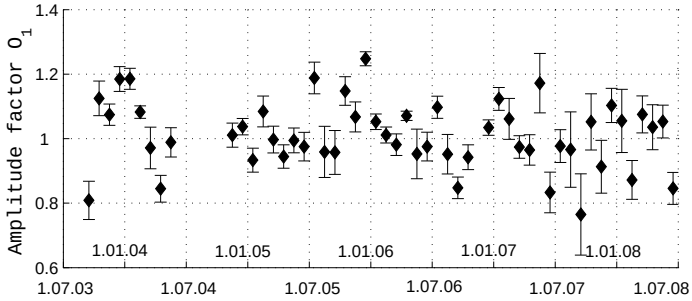

Figure 5. Amplitude factors for the tidal waves (a) M_2 and (b) O_1, calculated for monthly data. The vertical bars are rms deviation ranges.

correlated noise in the diurnal frequency range. In contrast, the M_2 wave, whose period differs significantly from both the nearest tidal components, N_2, L_2, S_2, and K_2 and from the average solar day, has a high signal-to-noise ratio and is therefore a main amplitude-phase indicator of the elastic response of the crust to the tidal action. The phase delay of the O_1 wave varies from $-5°$ to $+5°$ (the average over all time intervals is $-1.3°$). The determination uncertainty of the phase delay is $1°$ to $3°$. A quite stable phase delay for the M_2 wave varying from $0°$ to $1°$ (an average of $0.1°$) with a determination uncertainty of the order of $0.5°$ points to the absence of any systematic effects and to stable operation of the instrument. No appreciable seasonal variations are noted either.

The topography of the area in the immediate vicinity of the observation point appreciably distorts tidal strains. The effect of the topography on the amplitudes and phases of tidal tilts and strains was estimated by the perturbation method of a small parameter [9,10]. Using this method, the topography of the Baksan gorge was approximated by the 8th order polynomial (Fig. 6). The Baksan laser interferometer is located at a depth of about 400 m and is oriented along the axis perpendicular to the gorge. The direct calculation of perturbations associated with the effects of topography and the position of the interferometer yields a relative strain anomaly equal to +0.22. Thus, the topography effect increases the measured strain values by 22%.

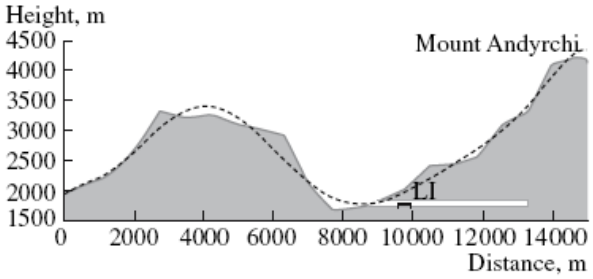

Figure 6. Approximation of the Baksan gorge topography along the cross section of the main gallery of the Baksan Neutrino Observatory (INR RAS) by a polynomial of degree 8. The position of the laser interferometer (LI) is shown.

4. Discussion of results of observation

Analysis reveals statistically significant temporal variations in the amplitude factors of the wave M_2 , while for the O_1 wave they are only scattered in time. The values of this factor lie within the range 1.02–1.15 (on average, 1.10) for M_2 and 0.76–1.24 (on average, 1.01) for O_1. In accordance with the estimated topography effect, we have to reduce the estimates of amplitude factors for the M_2 and O_1 waves by 22%. Therefore the mean values of the amplitude factors are 0.88 for M_2 and 0.81 for O_1. On the whole, the amplitude factors of the main diurnal and semidiurnal tidal waves are underestimated.

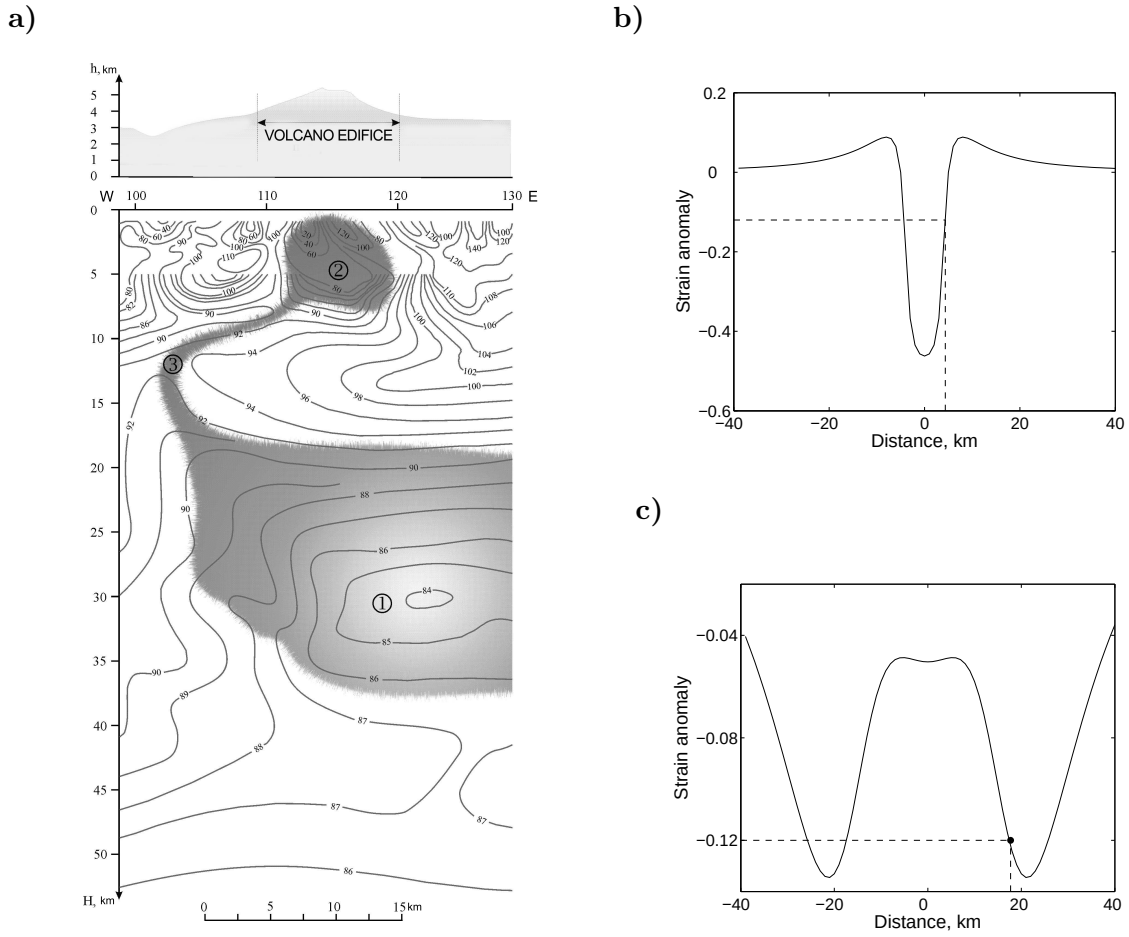

Figure 7. Influence of Elbrus magmatic structures on tidal strain amplitude: (a) Elbrus Volcano and its volcanic chambers from data on the tectonic fragmentation field [2]: (1) potential magma source; (2) shallow magma chamber; (3) a possible channel of primary magma flow. (b) and (c) the results of numerical modeling of anomalous effects of the magma chamber (b) and magma source (c).

Thus, the M_2 and O_1 anomalies of tidal strains average 12 and 19%, respectively. Since the topography effect is compensated, the observed anomalies are apparently associated with the presence of a large regional heterogeneous inclusion. The influence of such an inclusion can be estimated by analogy with the topography effect [9].

The nearest tectonic fault extends for 5 km from the Baksan laser interferometer station in the N–W direction, that is, almost parallel to an interferometer arm [7]. The anomalous strain caused by this fault is negligible. The magmatic structures of the Elbrus volcano can play the role of large regional heterogeneous inclusions because the Baksan laser interferometer is located at a distance of 18 km from its peaks. Modern technologies for processing space images of the Earth's surface identify near the Elbrus volcanic center two areas of anomalously low values of the tectonic fragmentation field of the lithosphere that are interpreted as a potential magma source and chamber of the Elbrus volcano [2]. The Elbrus magma chamber is located exactly beneath its volcanic edifice at depths from 1 to 8 km. The chamber width attains 9 km. The other tectonically weakened zone interpreted as a magma source is traceable from depths of 40–45 km up to 15–17 km (Fig. 7a). Results of the observations and analysis of regional resonance modes also reveal a shallow magma chamber in the structure of the Elbrus volcano [8].

Using a method proposed by Molodensky [9], we calculated anomalies of M_2 tidal strains in the vicinity of a soft inclusion in the shape of an infinite (along the horizontal Y axis) rectangular parallelepiped similar in cross-section dimensions and occurrence depth to the magma chamber and source. The results of numerical modeling are presented in Fig. 7b (chamber) and Fig. 7c (source). The anomalous effect of the magma chamber becomes rapidly weaker with distance from the volcano center and becomes negligible at a distance of 18 km (at the observation point); a tidal anomaly of 12% will be observed at a distance of 4.3 km. The tidal anomaly associated with the deep source varies with distance according to a more complex law and attains a value of 12% at distances of 18 km (at the observation point) and 26 km from the volcano center. Thus, the observed tidal strain anomaly is apparently due to the influence of the Elbrus deep magma source.

5. Estimation of the fluid core resonance effect

Free core nutation of the Earth causes the fluid core resonance (FCR) at the frequency of 1.0023 *cycles per sideral day*, which leads to disturbances of the tidal waves in the diurnal band. The FCR effect should deform essentially the amplitudes of tidal waves in a range of frequencies from 14.9 degree/h to 15.15 degree/h, that is, the waves K_1, Ψ_1 Φ_1. We have performed the preliminary analysis to estimate the influence of the FCR on the amplitudes of diurnal tidal harmonics. Three data sets were used from 2000 to 2007. The data were represented as 40 monthly segments. The analysis was done using `ETERNA` software, and the decomposition included 17 groups of waves: ten waves in the diurnal band (Q_1, O_1, NO_1, P_1, S_1, K_1, Ψ_1, Φ_1, J_1, OO_1), six waves in the semidiurnal band ($2N_2$, N_2, M_2, L_2, S_2, K_2), and the third diurnal wave M_3. The preliminary analysis also included correction of the strain data on three temperature channels, which was carried out using the program `TSOFT`. The results of the analysis are shown in Table 1. The analysis clearly reveals lunisolar declination wave K_1, for which the signal-to-noise ratio is more than 50. It is considered that all meteorological effects distort the diurnal

Table 1
Computed parameters of tidal waves according to 2002–07 strain data.

Wave	Ampl., nstr	Ampl. fac.	STDV	Phase Lead	STDV, (deg)
Q_1	0.958	0.9604	0.1227	0.01	7.32
O_1	5.362	1.0293	0.0235	-1.53	1.3
NO_1	0.452	1.1031	0.2987	4.69	15.51
P_1	2.228	0.9193	0.0504	-24.3	3.14
S_1	2.14	37.3351	2.1349	-4.68	3.27
K_1	6.213	0.8481	0.0167	-10.4	1.12
Ψ_1	0.159	2.7792	2.135	129.11	44.01
Φ_1	0.181	1.7306	1.1731	85.65	38.83
J_1	0.403	0.9831	0.2987	-12.13	17.41
OO_1	0.176	0.7867	0.5459	-9.01	39.75
$2N_2$	0.339	1.0518	0.1123	-7.03	6.12
N_2	2.19	1.0847	0.0179	0.82	0.94
M_2	11.553	1.0955	0.0034	-0.04	0.18
L_2	0.323	1.0849	0.1215	-4.84	6.42
S_2	5.226	1.0653	0.0073	0.95	0.39
K_2	1.438	1.0783	0.0271	1.65	1.44
M_3	0.065	1.1596	0.3145	14.57	15.541

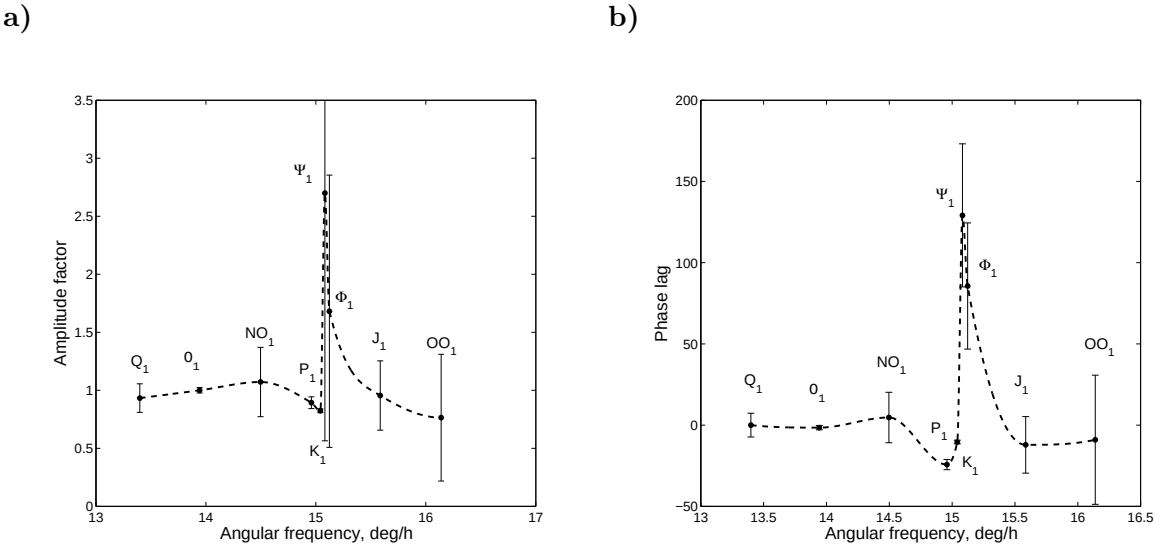

Figure 8. Fluid core resonance effect in the diurnal tidal band. Estimated amplitude factors (a) and phase lag (b) of the diurnal tidal constituents. Bars indicate *rms* errors.

constituents in the same way. To estimate the FCR effect, the wave O_1, which is far from resonance, is chosen as reference for near-resonance constituents. The amplitudes for K_1, Ψ_1 and Φ_1 constituents are 82%, 270%, and 168% of the amplitudes free from the FCR effect, respectively. The computed phase lags for these waves are $-10°$, $129°$, and $85°$, respectively. As it follows from the Table 1 the wave S_1 is very perturbed (the amplitude factor is 37). The minor constituents of the diurnal tidal bands, Ψ_1, and Φ_1, being harmonics of S_1, are obviously affected by S_1, that is expressed in the very large phase lags observed on Ψ_1, and Φ_1. Accuracies of the amplitude and phase estimations for these minor waves are very low. Fig. 8 demonstrates the influence of the FCR effect on the diurnal harmonics of tidal waves.

6. Conclusion

The principal finding of this study is the considerable anomalies in tidal wave amplitudes which are observed in the mountain area of the Northern Caucasus, near to the volcano Elbrus, one of the most geodynamically active regions of Russia. This result is based on long-term regular observations of tidal strains which were performed with the use of the Baksan laser interferometer strainmeter with a measuring arm length of 75 m mounted at a depth of 400 m below the Earth's surface. The data from 2003 to 2008 were used for the tidal harmonic analysis which was carried out using the `ETERNA` software package. The main semidiurnal wave M_2 is most reliably resolved by the analysis. For the one-month observation intervals, this tidal harmonic has a signal-to-noise ratio within the range 100–170 (280 at the most). The determination uncertainty of the amplitude factor is 0.5–1%. Thus, the M_2 wave is a main amplitude-phase indicator of the elastic response of the crust to the tidal action.

The topography of the area in the immediate vicinity of the observation point can appreciably distort tidal strain values. It is particularly important to take into account the topography in a mountainous area; in particular, inclination angles of the Baksan gorge profile attain 30–35°. The topography of the Baksan gorge at the location of the laser interferometer was approximated by a polynomial of degree 8. Direct calculations of tidal strain perturbations due to the topography effect yield a strain value of +0.22, which is larger than the measured strain values by 22%.

On the whole, the reduced amplitude factors of tidal waves are underestimated. The tidal strain anomaly averages 12% for M_2 and 19% for O_1. Tectonic faults and Elbrus magmatic structures can play the role of large regional heterogeneous inclusions distorting tidal strains. The nearest fault extends at a distance of 5 km from the location of the Baksan laser interferometer and is nearly parallel to its sensitive arm. However, the anomaly caused by this fault is negligible. In contrast, mathematical modeling of the anomalous effect caused by the magma source of Elbrus volcano shows that this effect can be appreciable. The tidal anomaly attains 12% at a distance of 18 km from the volcano center (at the observation point). Apparently we may suggest that the observed tidal strain anomaly is due to the influence of the deep magma source of the Elbrus volcano.

The existence of long-term observations allowed us to also estimate the FCR effect. This analysis is based on the data from 2000 to 2007. The computed amplitudes for

K_1, Ψ_1 and Φ_1 constituents are 82%, 270%, and 168% of the amplitudes free from the FCR effect, respectively. The FCR effect analysis is considered to be a preliminary one. We hope to improve the estimation of near-resonance constituents and to estimate the parameters of free core nutation of the Earth in a future study.

7. Acknowledgments

This work was supported by the *Russian Foundation for Basic Research*, project No.07-05-13573-ofi_c and No.07-05-00786-a.

REFERENCES

1. Bogatikov, O.A., Nechaev, Yu.V., Sobisevich, A.L., 2002a. The use of cosmic technologies for the monitoring of geological structures of Elbrus volcano. Dokl. Akad. Nauk. 387 (3), 364–369.
2. Bogatikov, O.A., Gurbanov, A.G., Rogozhin, E.A., et al., 2002b. Activation of Elbrus volcano and its possible consequences. In: Catastrophic processes and their implications for the environment, vol. 1: Volcanism, IFZ RAN, Moscow, 346–397.
3. Dziewonski, A.M., Anderson, D.L., 1981. Preliminary reference Earth model. Phys. Earth Planet. Int. 25, 297–356.
4. Melchior P., 1966. The Earth Tides. Pergamon Press, Oxford.
5. Milyukov, V.K., Klyachko, B.S., Myasnikov, A.V., Striganov, P.S., Yanin, A.F., Vlasov, A.N., 2005. A laser interferometer - deformograph for monitoring the crust movement. Instr. Exp. Techniques. 48 (6), 780–795.
6. Milyukov, V.K., Myasnikov, A.V., 2005. Metrological characteristics of the Baksan laser interferometer. Izmerit. Tekhnika. No. 12, 26–30.
7. Kopaev, A., Milyukov, V., 2002. Environmental effects in tide strain observations near the mt. Elbrus, Central Caucasus. Marees Terrestres. Bull. d'Inform. 137, 10909–10916.
8. Milyukov, V.K., 2006. Monitoring of the state of Elbrus magmatic structures using lithospheric strain observations. Vulkanol. Seismol. No. 1, 3–15.
9. Molodensky, S.M., 1983. Determination of tidal strain perturbations for a plain topography. Izv. AN SSSR, Ser.Fiz. Zemli, No. 7, 80–96.
10. Molodensky, S.M., 1986. The plain topography implications for tidal tilts and strains: effects of second order. Izv. Akad. Nauk SSSR, Ser. Fiz. Zemli, No. 8, 3–14.
11. Rogozhin, E.A., Sobisevich, L.E., Nechaev, Yu.V., et al., Geodynamics, Seismotectonics, and Volcanism of the Northern Caucasus. 2001. IFZ RAN, Moscow.